Carrier Recombination Dynamics of Surface Passivated Epitaxial (100)Ge, (110)Ge, and (111)Ge Layers by Atomic Layer Deposited Al_2O_3

Mantu K. Hudait[*,†], Steven W. Johnston[‡], Manash R. Das[‖,§], Sengunthar Karthikeyan[†], Partha P. Sahu[⊥], Jagat Das[⊥], Jing Zhao[±], Robert J. Bodnar[±], and Rutwik Joshi[†]

[†]Advanced Devices and Sustainable Energy Laboratory (ADSEL), Bradley Department of Electrical and Computer Engineering, Virginia Tech, Blacksburg, Virginia 24061, USA

[‡]National Renewable Energy Laboratory, Golden, Colorado 80401, USA

[‖]Materials Sciences and Technology Division, CSIR-North East Institute of Science and Technology, Jorhat - 785006, Assam, INDIA

[§]Academy of Scientific and Innovative Research (AcSIR), Ghaziabad 201002, India

[⊥]School of Engineering, Department of Electrical and Computer Engineering, Tezpur University, Napaam, Tezpur-784028, Assam, INDIA.

[±]Fluids Research Laboratory, Department of Geosciences, Virginia Tech, Blacksburg, Virginia 24061, USA

ABSTRACT: Germanium (Ge) and its heterostructures with compound semiconductors offer a unique optoelectronic functionality due to its pseudo-bandgap nature, that can be transformed to a direct bandgap material by providing strain and/or mixing with tin. Moreover, two crystal surfaces, (100)Ge and (110)Ge, that are technologically important for ultra-low power fin or nanosheet transistors, could offer unprecedented properties with reduced surface defects after passivating these surfaces by atomic layer deposited (ALD) dielectrics. In this work, the crystallographically oriented epitaxial Ge/AlAs heterostructures were grown and passivated with ALD Al_2O_3 dielectrics, and the microwave photoconductive decay (μ-PCD) technique was employed to evaluate carrier lifetimes at room temperature. The x-ray photoelectron spectroscopy analysis reveals no role of orientation effect to the quality of ALD Al_2O_3 dielectric on oriented Ge layers. The carrier lifetimes measured using μ-PCD technique were benchmarked against unpassivated Ge/AlAs heterostructures. Excitation wavelength of 1500 nm and 1800 nm with an estimated injection level of ~ 10^{13} cm^{-3} were selected to measure the orientation-specific carrier lifetimes. The carrier lifetime was increased from 390 ns to 565 ns for (100)Ge and from 260 ns to 440 ns for (110)Ge

orientations with passivation, whereas the carrier lifetime is almost unchanged for (111)Ge after passivation. This behavior indicates a strong dependence of the measured lifetime on surface orientation and surface passivation. The observed increase (>1.5 ×) in lifetime with Al_2O_3 passivated (100)Ge and (110)Ge surfaces is due to the lower surface recombination velocity compared to unpassivated Ge/AlAs heterostructures. The enhancement of carrier lifetime from passivated Ge/AlAs heterostructures with (100) Ge and (110)Ge surface orientations, offer a path for the development of nanoscale transistors due to the reduced interface state density.

KEYWORDS: *Germanium, Al_2O_3, Molecular Beam Epitaxy, X-ray Photoelectron Spectroscopy, Lifetime, atomic layer deposition*

1. INTRODUCTION

Group-IV materials (*i.e.*, Ge, GeSn, SiGeSn, SiGe) exhibit a potential application in line with quantum science and technology, due to their unique spintronic and optoelectronic functionalities valuable for qubits.[1-15] By exploiting strain and bandgap engineering of these materials *via* intelligent buffer engineering[1-4] and precise control of tin (Sn) composition in GeSn or SiGeSn during materials synthesis,[8,9,11-13, 15] it will offer widespread applications in Si-compatible photonics and quantum technology, provided that one could synthesize device-quality group-IV materials. In addition, downscaling of silicon (Si) transistors was possible by changing the device geometry from planar to fin field effect transistors (FinFETs). Researchers are now looking into gate-all-around nanosheet FETs (NSFETs) [16-22] and high-mobility Ge channel material, to maintain transistor ON current, while reducing supply voltage and footprint. [16-22] In the former, crystallographic planes of (100)Si and (110)Si along with HfO_2-based high-κ gate dielectrics were used for high-performance, low-power Si CMOS logic down to N3 technology node,[20, 21] enabling increased integration of complex functionality on a single die. The integration of high-κ gate dielectrics such as HfO_2, Al_2O_3 on (100) and (110) crystal planes should not produce defects due to the effect of process temperature during deposition, rather only passivating the surface states and eliminate the interdiffusion of high-κ dielectric and channel materials.[23, 24] Using these technologically important crystal planes, (100) and (110), from high electron and hole mobility Ge channel materials compared with Si[25] along with high-κ dielectric, one could make FinFET[26, 27] or gate-all-around (GAA) NSFET[16-23] for high density and ultra-low power CMOS. However, the interfacial defects at the high-κ (*e.g.*, HfO_2) and Ge channel material would require an interface passivation layer (IPL) to control the interface state density (D_{it}).[26, 27] *In-situ* ultra-thin SiO_2 passivation layer from tris(tert-butoxy)silanol ($Si(OH)(OC\text{-}(CH_3)_3)_3$) precursor during atomic layer deposited (ALD) gate dielectric[28] or by Si IPL layer and/or GeO_x *via* thermal oxidation or by ozone oxidation was prescribed as IPL layer formation strategies for subsequent Al_2O_3 and composite Al_2O_3/HfO_2 dielectrics deposition.[26-44] In either case, the main objective was to reduce the D_{it} at the high-κ/Ge heterointerface. Over the last two decades, surface recombination velocities (SRV) ≤ 1 cm/s were reported for Si[45-48] and ultra-low SRV values were made possible by superior surface passivation with low D_{it} ≈10^9-10^{12} $eV^{-1}cm^{-2}$.[29-44] The extensive research on the surface passivation of Si with low D_{it} over the

decades has been transferred to *p*-Ge and *n*-Ge by several researchers.[45-47] Noticeably, Berghuis *et al.*[39] have studied the surface passivation of bulk-Ge using a combination of plasma enhanced ALD (PEALD) and thermal ALD a-Si:H/Al_2O_3 as well as PEALD Al_2O_3 stack and achieved SRV as low as 2.7 cm/s. The $D_{it} \approx 1\times10^{12}$ $eV^{-1}cm^{-2}$ was determined from capacitance-voltage measurements of PEALD Al_2O_3/Ge metal-oxide-semiconductor capacitor. In addition, the relationship between SRV and carrier lifetime (τ_{eff}) is given by,

$$\frac{1}{\tau_{eff}} = \frac{1}{\tau_B} + \frac{2S}{d},$$

where, τ_B is the bulk lifetime, *d* is the thickness of the layer of interest, and *S* is the SRV. Thus, high carrier lifetime characterizes reduced loss of accumulated/inverted carriers due to recombination at the high-κ/Ge heterointerface, which is essential during the fabrication of a NSFET either from Si or Ge or GeSn. In this NSFET structure, high-κ dielectric by ALD is required to form a conformal growth along the four sides of a nanosheet transistor,[16-22] where the two (100) and two (110) crystal planes form a NSFET similar to two (110) and one (100) crystal plane form a trigate/FinFET device,[26, 27] and **Fig. 1** shows the schematic representation of a Ge FinFET structure on GaAs or Si substrate. During the ALD deposited gate dielectric, such as Al_2O_3 on these crystal planes, one must maintain the low D_{it} [29-31] by decreasing reduced surface states and probing each passivated Al_2O_3/(100)Ge and Al_2O_3/(110)Ge heterointerface recombination properties related to the carrier lifetime, would offer valuable information to the scientific community as well as an impactful technological contribution. The carrier lifetime is widely acknowledged as an important parameter used in the evaluation of material and interface quality due to its sensitivity to defects, where ALD deposited high-κ dielectrics is considered to be a potential solution for reducing those surface defects by passivating the surface states of a semiconductor.[29-44] Indeed, several studies related to bulk Ge or Ge on Si surface passivation by ALD Al_2O_3, reported an improvement in the carrier lifetime by ~ 1.8 × over unpassivated Ge[38, 39, 49] at room temperature. This suggests that the surface passivation of

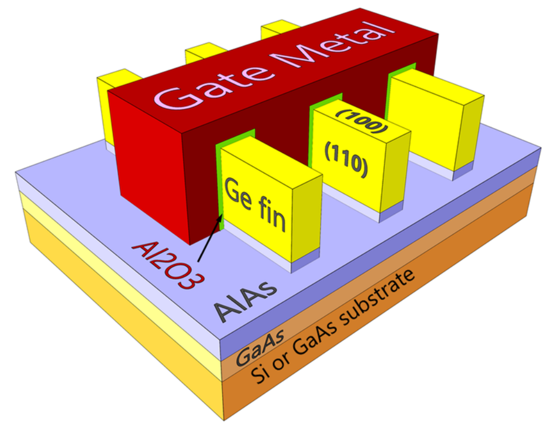

Figure 1. Schematic representation of Ge FinFET structure on GaAs or Si substrate with an intermediate AlAs buffer layer, where (100)Ge and (110)Ge crystal planes were used to form FinFET device structure.

oriented Ge by ALD Al_2O_3 dielectric, and probing the carrier lifetime of Ge surfaces would provide information related to SRV and D_{it} for forward looking research on Ge or GeSn based transistors.

The man-made (100) and (110) or naturally occurring crystal surfaces can exhibit different electronic and photonic properties[49-58] with different carrier lifetime on those surfaces. The carrier recombination properties from the crystallographically oriented (100)Ge, (110)Ge, (111)Ge were demonstrated,[50, 53, 55] where the (111)Ge surface exhibited low carrier lifetime compared to other orientations. It was believed to be the defect states within the bulk responsible for the low carrier lifetime for (111)Ge plane. In addition, it was also not clear whether the surface states or metallic nature of this crystal plane is responsible for the low carrier lifetime from this study.[50] However, the different surface trap states were reported within the Si[52] and Ge[53-55] semiconductors, and the density of the surface states (N_{SS}) in Ge related to its crystallographic orientations, varies as $N_{SS}\langle 111\rangle < N_{SS}\langle 110\rangle < N_{SS}\langle 100\rangle$.[53, 55] However, the (111)Ge surface exhibited high electrical conductivity leading to short carrier lifetime compared to other orientations.[53-55] If the (111)Ge surface is passivated with ALD Al_2O_3, where trimethylaluminum (TMA, $Al(CH_3)_3$) was used as the metal precursor, then the carrier lifetime should improve from the passivated Al_2O_3/(111)Ge heterostructure along with other orientations. Hence, this will shed more light on the orientation-specific carrier lifetimes of Al_2O_3 passivated different crystal planes of Ge layers.

In this work, we have measured the carrier lifetimes from Al_2O_3 passivated epitaxial (100)Ge, (110)Ge, and (111)Ge layers, and the measured results were compared with unpassivated (as-grown) crystallographically oriented Ge layers. These Ge layers were grown on different oriented GaAs substrates to create an orientation-specific epitaxial layer by solid source molecular beam epitaxy (MBE). An approximately 10 nm thick ALD Al_2O_3 layer was deposited on 3 different oriented Ge layers in order to observe the effect of surface passivation by TMA and de-ionized water (DI H_2O) as oxygen source. Selected epitaxial layers with and without Al_2O_3 were characterized by x-ray photoelectron spectroscopy (XPS) to determine the depth profile of each element and the binding energy distribution curves of their core level (CL) states. Finally, the carrier lifetime of unpassivated (*i.e.*, without Al_2O_3) and Al_2O_3 passivated (100)Ge, (110)Ge, and (111)Ge epitaxial layers were probed by microwave photoconductive decay (μ-PCD) method at two different excitation wavelengths, 1500 nm and 1800 nm. The μ-PCD data displays carrier lifetimes of 65 ns to 540 ns for orientation-specific Ge layer, indicating a strong dependence on surface

orientation and surface passivation. Thus, the orientation-specific carrier lifetime in Al_2O_3 passivated Ge layers would have a prospect for future development of Ge-based nanosheet transistors[20, 21] and nanoscale fin transistors.[20, 26, 27]

2. EXPERIMENTAL SECTION

2.1. Materials synthesis. Crystallographically oriented (100)Ge, (110)Ge, and (111)Ge layers were grown *in-situ* using dual chamber (one for group III-V and another for group-IV semiconductors) vacuum interconnected MBE system on AXT Inc made epi-ready 2° offcut (100)GaAs, (110)GaAs and (111)A GaAs substrate, respectively. An *in-situ* reflection high energy electron diffraction system attached to the group III-V growth chamber was used to monitor each GaAs substrate oxide desorption, surface reconstruction of GaAs and AlAs layers as well as the entire growth process. Arsenic valved cracker source for As_2 flux and SUMO® effusion cells for Ga, Ge, and 60 cc capacity of Al cells were used for growing layered structures. The arsenic bulk and cracker temperatures were kept at ~340°C and 900°C, respectively, in order to maintain the over pressure of As_2/Ga or As_2/Al ratio > 22. Each GaAs substrate oxide desorption was performed at ~750°C under As_2 over pressure of ~10^{-5} torr. The temperature referred to here is the thermocouple temperature. After the oxide desorption of each GaAs wafer, the substrate temperature was reduced to 650°C for (100)GaAs, 600°C for (110)GaAs, and 550°C (111)GaAs for 250 nm thick GaAs layer growth and at a growth rate of 0.5 µm/hr. The growth temperature for the (100)GaAs is higher than other crystallographic orientations due to the surface adatom mobility.[59] After each GaAs layer growth, an ~200 nm thick AlAs layer was grown on each oriented GaAs substrate at ~670°C. Upon completion of the AlAs/GaAs growth within the group III-V chamber, each sample was cooled down below 200°C under As_2 flux before being transferred to the group-IV chamber for Ge layer growth. The growth temperature was kept constant at 400°C for each Ge layer growth and the thickness of each Ge layer was ~280-290 nm, and the growth rate of Ge was ~ 0.1 Å/s. The 400°C growth temperature of Ge was selected in order to prevent the indiffusion of Ge into AlAs and outdiffusion of Al and As into Ge film. This process demonstrated a 6 Å abruptness at the Ge/AlAs heterointerface by atom probe tomography.[60] After the Ge layer growth, each sample was slowly cooled to < 100°C to avoid thermal cracking and kept inside the ultra-vacuum (~2×10^{-10} torr) buffer chamber. Further details of the

growth process have been reported earlier.[59] The carrier density of the unintentionally doped Ge layer (*n*-type) is in the range of 2-4×10^{18} cm^{-3}, reported earlier.[61]

A Cambridge NanoTech ALD reactor was used for the deposition of ~10 nm Al_2O_3 on each crystallographically oriented Ge layer using TMA and DI H_2O as the oxygen source, and a growth temperature of 250°C. All three oriented Ge layers were placed at the same time inside the ALD reactor for Al_2O_3 deposition. The Al precursor was kept at room temperature and the entire line (exit port of Al precursor to entry port of reactor) was heated to a temperature of ~ 150°C to prevent deposition inside the tube. Prior to loading into the ALD reactor for Al_2O_3 deposition, each sample surface was treated with a standard solvent cleaning using acetone, isopropanol, and de-ionized water, followed by a 60 s native oxide removal in a pre-mixed 10:1 buffered oxide (HF) etchant solution. Once the sample was loaded into the ALD reactor, the system was pumped down and purged with ultra-high pure nitrogen prior to the deposition of Al_2O_3. Each TMA pulse of 0.020 sec duration, which is ~1 Å/s growth rate was used for the deposition of 10 nm thick Al_2O_3 layer.

2.2. Materials analysis. Characterization of the crystallographic orientation of (100)Ge, (110)Ge and (111) Ge epitaxial layers was carried out using high-resolution x-ray analysis using a PANalytical X'pert Pro system equipped with PIXcel and proportional detectors, and a monochromatic Cu Kα (λ =1.540597 Å) X-ray source. The orientation of each Ge layer was identified by selecting the GaAs Bragg angle of reflection (ω) and the tilt (Chi) of each sample during measurement. The "Chi" in PANalytical X'pert Pro system denotes the angle between the surface plane of the sample and the crystallographic reflection plane under observation {here, (004)}. When identifying orientation, the angles between the crystallographic planes in the cubic Ge crystal structure are important. For example, the angle between (100) and (110) plane is 45°, and (100) and (111) is 54.7°. During x-ray measurement setup, the parameter "Chi" in PANalytical X'pert Pro instrument (diffractometer setting) was set for the samples a1 {(100)/2°Ge}, b1 {(110)Ge}, and c1 {(111)Ge} as 2.16°, 44.94°, and 54.73° respectively, which is in agreement with the theoretical values. Under these conditions, the GaAs substrate ω = 33.028° is almost matched for all orientations and each oriented Ge layer was identified by x-ray analysis. Detailed x-ray analysis of these structures were reported in earlier publication.[59] Cross-sectional transmission electron microscopy (TEM) analyses

of metal/Al_2O_3/(100)Ge and metal/Al_2O_3/(110)Ge samples were performed where metal was deposited for MOS capacitor studies. TEM analysis was not carried out on (111)Ge orientation due to the low carrier lifetime even after passivation, discussed below. However, the carrier lifetimes were determined from a separate set of samples, where metal contact was not deposited on top of Al_2O_3 gate oxide of each oriented sample, and this set of samples was used for XPS analysis at the research facilities of CSIR-North East Institute of Science and Technology, India. The JEOL 2100 transmission electron microscope was used for TEM analysis. Standard sample preparation techniques, i.e., mounting, polishing, and ion milling, were used to prepare electron transparent foil for TEM imaging. XPS Microprobe equipped with a monochromatic Al-Kα x-ray source (beam energy of 1486.7 eV) was used in the investigations (ESCALAB Xi^+, Thermo Fisher, UK). Samples were mounted on a plane surface where the angle between the x-ray source and the analyzer is 90º. The photoelectron exit angle during measurement was 24º. In order to neutralize the positive charge accumulation, especially on the oxide surface (this is a necessary requirement for an insulator with no conducting path while recording the XPS spectra) due to photoelectron generation (electron loss) during measurement, a low-energy electron flood gun was used throughout the measurement. The C 1s CL binding energy located at 284.8 eV correction was not made since relative intensity of each atomic species as a function of depth was given priority over the carbon correction of each peak position. Furthermore, the core level aluminum (Al 2p), germanium (Ge 3d, Ge 2p), gallium (Ga 3d), arsenic (As 3d), and oxygen (O 1s) spectra were recorded during the measurement for each crystallographic orientation. Raman spectra were collected in the (001) backscattering geometry using a JY Horiba LabRam HR800 system with spectra collected from crystallographically oriented Ge layers as well as from bulk Ge (control sample). The excitation wavelength of 514.48 nm (green) was provided by a Laser Physics Ar^+ laser and gratings with 1800 lines/mm were used during measurement. The laser power at the sample surface was ~7 mW. Spectra for all the epitaxial Ge layers and the bulk Ge were collected at the same time.

The microwave photoconductive decay (μ-PCD) method[62] at the National Renewable Energy Laboratory (NREL) was used to determine the carrier lifetime of ALD Al_2O_3 passivated and unpassivated oriented Ge layers. Laser excitation wavelengths of 1500 nm (0.83 eV) and 1800 nm (0.69 eV) at 20 mW laser power (measured by a power meter) were used to change the sample conductivity due to the excess carriers generated by laser excitation

as monitored *via* the microwave power reflected from each sample surface. The laser excitation was provided from the top on each sample surface (*i.e.*, Ge) that faces up during measurement. Each sample with dimensions of ~ 10 mm × 10 mm was placed directly under a waveguide (WR42 for 20 GHz, dimension of ~ 4.3 mm ×10.7 mm). The microwave signal fills the waveguide during each measurement. The laser pulse repetition rate was 10 pulses/sec with 5 ns pulse width and the laser beam spot was 20 mm in diameter. A glass slide with transparent conductive oxide was placed on top of the waveguide such that microwave power would reflect downward instead of radiating out from the top. A balsa wood sample stage was used during sample loading and unloading in each measurement. Using the above measurement parameters, the injection level of carriers was ~ 10^{13} cm^{-3} without considering the surface reflection and wavelength dependent absorption. The μ-PCD lifetimes were quantified for each oriented sample, corresponding to ~3 ns after the optical excitation pulse was ended. The curve fittings were performed using Origin 2022b software to determine the μ-PCD lifetimes. The details of this measurement technique can be found in Ref. [62].

3. RESULTS AND DISCUSSION

3.1. Heterointerface analysis via XPS.

Epitaxial Ge layers with different crystallographic orientations, shown in **Figs. 2a1**, **b1**, and **c1**, were grown on AXT Inc produced oriented GaAs substrates with an intermediate AlAs buffer layer using a vacuum interconnected, dual chamber (one for group III-V and another one for group-IV materials) Veeco Gen-II MBE growth system. The AlAs layer in each system was used to suppress or block interdiffusion of atomic species As, Ge, and Ga.[63] After the deposition of Al_2O_3 high-κ dielectric on (100)Ge, (110)Ge, and (111)Ge layers, the atomic depth profiling was carried out with

(a1)	(b1)	(c1)
(100) Ge 280 nm	(110) Ge 290 nm	(111) Ge 290 nm
AlAs 200 nm	AlAs 200 nm	AlAs 200 nm
GaAs 250 nm	GaAs 250 nm	GaAs 250 nm
(100)/2° GaAs substrate	(110) GaAs substrate	(111)A GaAs substrate

(a2)	(b2)	(c2)
Al_2O_3 10 nm	Al_2O_3 10 nm	Al_2O_3 10 nm
(100) Ge 280 nm	(110) Ge 290 nm	(111) Ge 290 nm
AlAs 200 nm	AlAs 200 nm	AlAs 200 nm
GaAs 250 nm	GaAs 250 nm	GaAs 250 nm
(100)/2° GaAs substrate	(110) GaAs substrate	(111)A GaAs substrate

Figure 2. Schematic representation of layer structures: (a1-c1) -unpassivated samples and (a2-c2) - Al_2O_3 passivated samples, where (a1) (100)Ge on AlAs/GaAs; (b1) (110)Ge on AlAs/GaAs; (c1) (111)Ge on AlAs/GaAs; (a2) 10 nm Al_2O_3/(100)Ge; (b2) 10 nm Al_2O_3/(110)Ge; and (c2) 10 nm Al_2O_3/(111)Ge.

samples (**a2–c2**) and samples (**a1–c1**) having no dielectric on top of each Ge layer by *ex-situ* XPS technique using Axis Ultra DLD x-ray photoelectron spectrometer in order to reveal the structure and chemical states of constituent elements as well as the distribution of atomic composition and impact of dielectrics on each oriented Ge (**Fig. 3**).

Ex-situ XPS measurements were carried out to evaluate the atomic distribution of elements within each structure. The Ar^+ ion gun (energy ~ 1 kV) within the XPS chamber was used to sputter three crystallographically oriented Ge samples (**a1-c1**). **Fig. 3** shows the XPS depth profiles of Ge, Al, Ga and As in each structure. In all cases, oxygen O 1s and carbon C 1s CL peaks from the surface of each structure were sputter-eliminated, where one can find the Ge atomic level is slightly lower than 100%. The depth scale was calibrated using the thickness of Ge and AlAs layers by cross-sectional TEM analysis with an estimated error of ~10%. In all cases, a constant Ge, Al, Ga, and As depth profile within each layer was observed, indicating good uniformity. Within the sputter-induced artifacts, varying escape depth of each element and XPS artifact due to the change of matrix element (Ge, Al, Ga, and As) transient effect, the depth profiles displayed smooth Ge/AlAs/GaAs heterointerfaces, studied in this work.

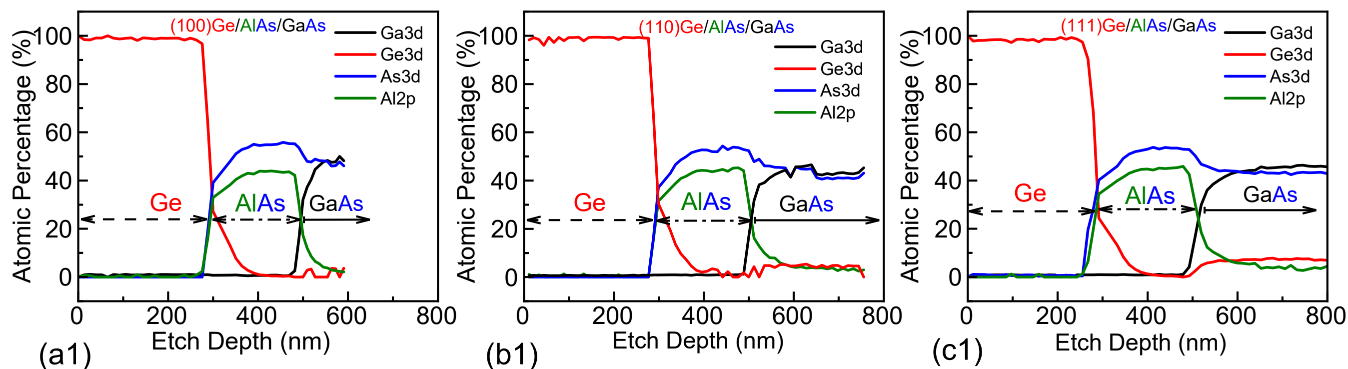

Figure 3. XPS depth profiles of Ge 3d, Al 2p, Ga 3d, and As 3d as a function of depth for three oriented Ge layers: (sample a1) (100)Ge, (sample b1) (110)Ge and (sample c1) (111)Ge.

3.2. Heterointerface analysis via cross-sectional TEM. Cross-sectional TEM analyses were performed on selected samples to corroborate the XPS depth profile analysis of **Fig. 3**, above. **Fig. 4** shows the TEM micrographs of Al_2O_3 on (100)Ge and (110)Ge oriented layers, where each layer is clearly shown in this figure. The apparent bending at the oxide/(100)Ge heterointerface in **Fig. 4(a)** corresponds to the measurement artifact induced during the preparation of TEM specimen. The sharp heterointerface of Ge/AlAs and abrupt heterointerface of oxide on (110)Ge was observed from **Fig. 4(a)-(b)** and **(c)**, respectively. One can also find uniform thickness of Al_2O_3 on Ge

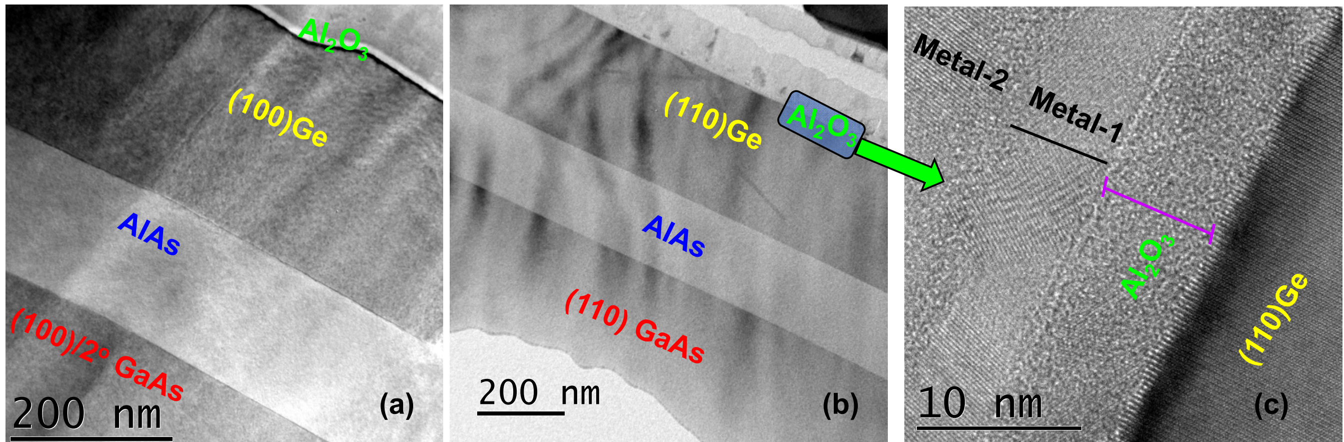

Figure 4. Cross-sectional TEM micrographs of atomic layer deposited Al_2O_3 on (a) (100)Ge, (b) (110)Ge and (c) high-resolution heterointerface of oxide and (110)Ge. Metals contact were deposited on samples for MOS-C studies.

layer by atomic layer deposition, which will passivate the surface defects or surface states on each Ge layer by improving the carrier lifetime measured by μ-PCD, discussed later.

3.3. Al_2O_3/(100)Ge, (110)Ge, and (111)Ge sputter depth-dependent analysis via XPS. **Fig. 5** displays the peak evolution of Al 2p and O 1s CLs as a function of sputter depth obtained from the Al_2O_3 passivated (100)Ge, (110)Ge,

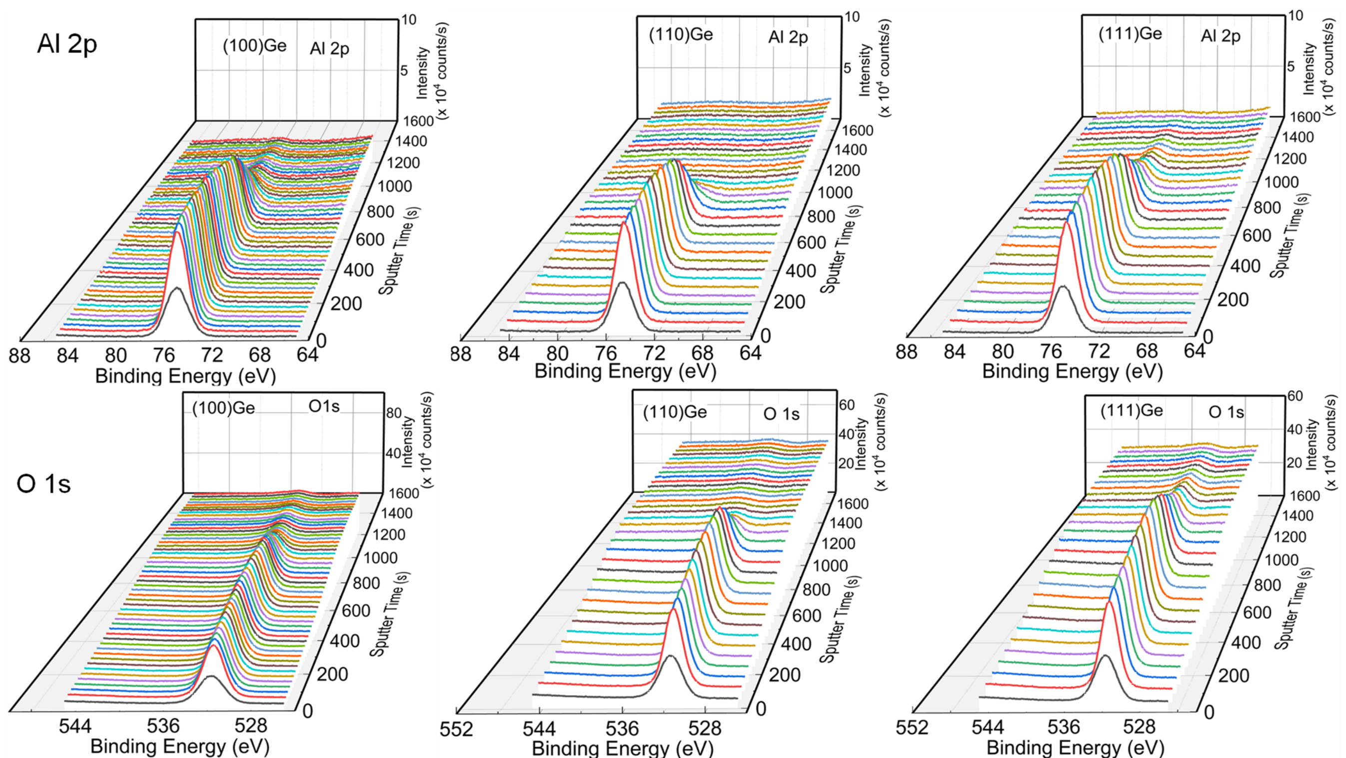

Figure 5: Sputter depth-dependent analysis of Al 2p and O1s core level spectra obtained from Al_2O_3 passivated (100)Ge, (110Ge, and (111)Ge (samples **a2**, **b2**, and **c2**) layers.

and (111)Ge layers. The depth dependent analysis of Ge 3d and Ge 2p CL spectra obtained from Al_2O_3 passivated (100)Ge and expanded view from 700 to 1000 sec, shown in **Fig. 6**. **Fig. 7** shows the sputter depth-dependent analysis of Ge 3d and Ge 2p core level spectra obtained from Al_2O_3 passivated (110Ge and (111)Ge (samples **b2** and **c2**) layers. These CL spectra were collected during XPS measurements using Ar^+ ion gun sputtering, with 25 sec periodicity for (100)Ge, and 50 sec for both (110)Ge and (111)Ge, respectively, as a function of time. We can demarcate that at the sputtered time of ~ 800 sec, the Al 2p and O 1s CL peak intensity level decreases and the Ge 3d CL peak intensity increases with sputtering time, as expected. As the escape depth of the Ge within Al_2O_3 is ~ 1.8 nm,[64] one can start observing the Ge peak prior to the decay of the Al 2p and O 1s CL spectra, as shown in **Fig. 5**. Due to this,

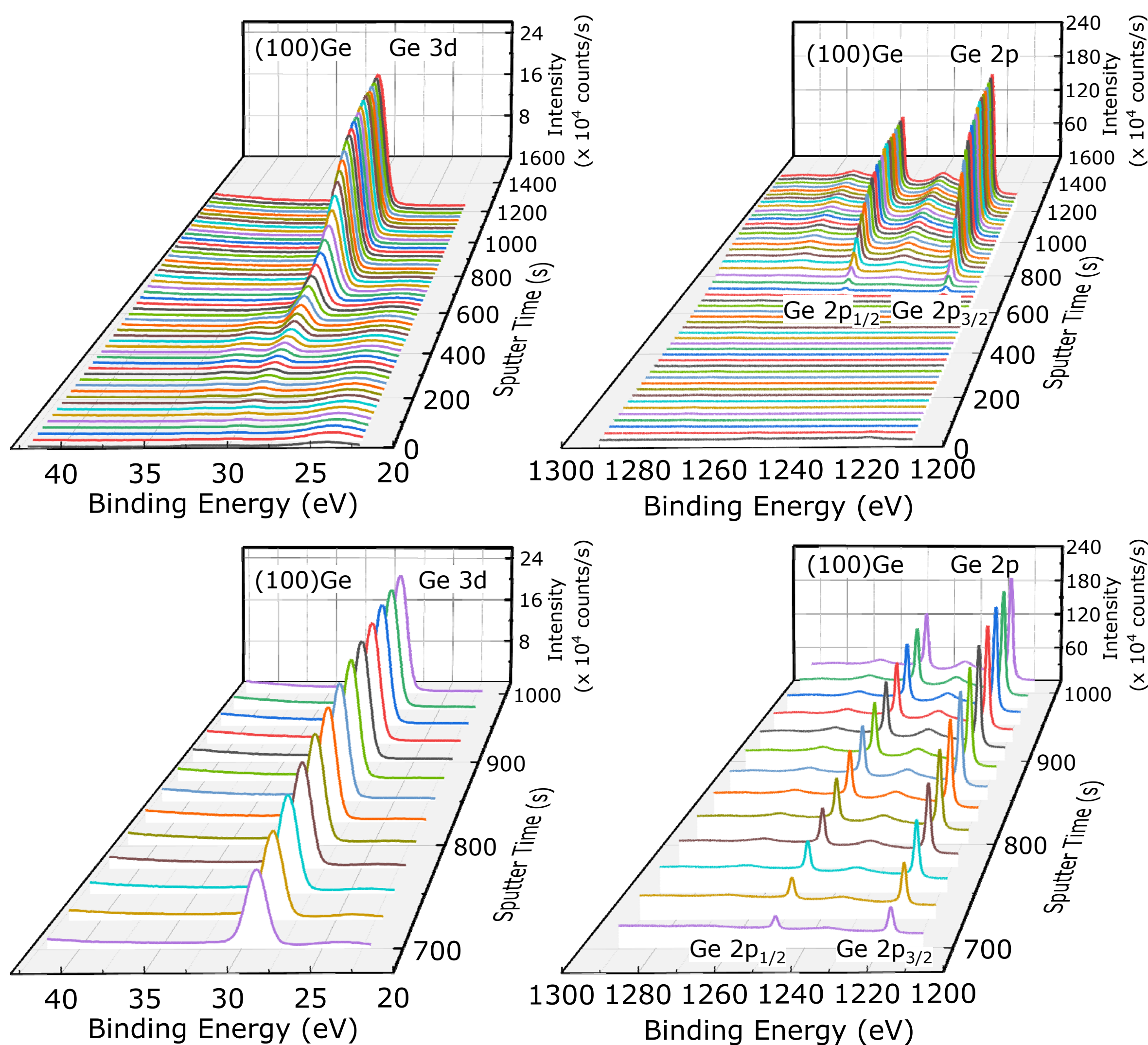

Figure 6: Sputter depth-dependent analysis of Ge 3d and Ge 2p core level spectra obtained from Al_2O_3 passivated (100)Ge (samples **a2**) layer and expanded view from 700 to 1000 sec.

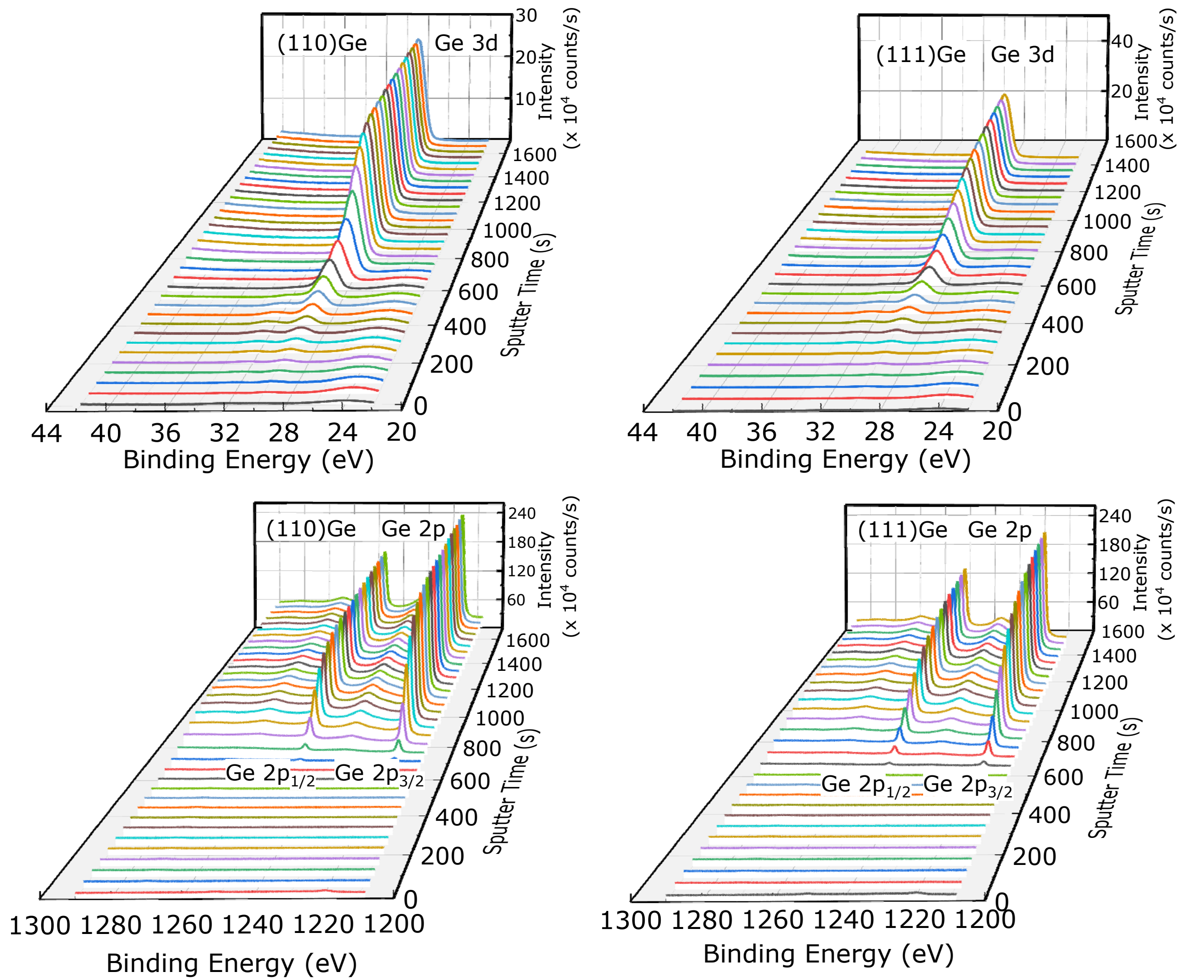

Figure 7: Sputter depth-dependent analysis of Ge 3d and Ge 2p core level spectra obtained from Al_2O_3 passivated (110Ge and (111)Ge (samples **b2** and **c2**) layers.

the exact position of Al_2O_3/Ge heterointerface from the sputter depth spectra cannot be ascertained with high precision. In addition, there is no apparent distinction of these peaks from three oriented Al_2O_3/Ge layers. **Fig. 8** shows the XPS depth profiles of Al 2p, O 1s, and Ge 3d peaks as a function of depth and these peak positions were obtained from **Fig. 5**. The elemental composition of the ~10 nm Al_2O_3 dielectric can be obtained from the ratio of atomic percentage of O to Al: [O/A] = 1.53 ± 0.05 eV, indicating good quality of the Al_2O_3 dielectric by ALD on three oriented Ge layers. Differences in the composition ratio of O 1s to Al 2p are not observed in **Fig. 8**, indicating there is no role of orientation effect to the Al_2O_3 dielectrics.

The ALD deposited Al_2O_3/Ge interface is of high quality and formed without any unintended stoichiometric or sub-stoichiometric GeO_x formation (**Fig. 5**). There is no observed chemical shift in the Ge 3d, Ge $2p_{3/2}$ or Ge $2p_{1/2}$

CL binding energy peaks. Absence of chemically shifted peaks in the neighborhood of Ge 3d and Ge 2p binding energy ranges show that within this periodic sputtering of 25 secs, neither Ge 3d nor Ge 2p CL states were oxidized to any stoichiometric or sub-stoichiometric GeO_x. In the case of GeO_x formation, one should detect multiple peaks on the higher binding energy region (>1249 eV for Ge $2p_{1/2}$) of each Ge CL peak. Their absence supports the good quality of the Al_2O_3/Ge heterointerface,[65] as per the current ALD deposition needs, beginning with the emergence of the Ge CL peaks as we sputter down from the Al_2O_3 dielectric to reach to the Ge epilayer. The smaller humps (around 1234.8 eV and 1265.8 eV) on higher binding energy side of Ge $2p_{3/2}$ and Ge $2p_{1/2}$, respectively, are the energy loss lines with spin orbit splitting difference of ~ 31 eV. Also, the earlier emergence of the Ge 3d CL peak (around 400 sec) compared to both Ge $2p_{3/2}$ and Ge $2p_{1/2}$ peaks (around 650 sec) with sputter duration indicates the deeper CL and stronger binding energy distribution nature of Ge 2p CL compared to Ge 3d CL (that has higher mean escape depth than Ge 2p). These passivated Al_2O_3/Ge structures were further evaluated by μ-PCD to determine the carrier lifetimes to study their effects on oriented Ge, as discussed later.

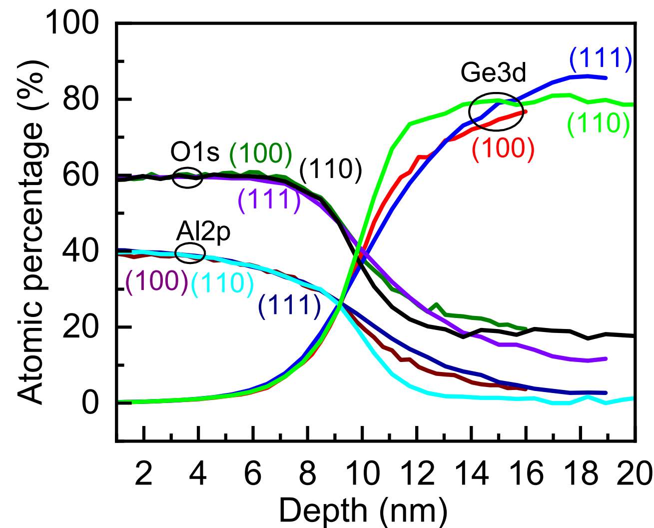

Figure 8: XPS depth profiles of 10 nm thick ALD Al_2O_3 on crystallographically oriented (100)Ge, (110)Ge and (111)Ge layers (samples **a2**, **b2**, and **c2**).

3.4. Ge vibrational properties via Raman spectroscopy. Raman spectroscopy analysis of semiconductor materials widely used by the semiconductor industry to determine the strain and compositional analysis of SiGe source-drain for several decades. In this work, Raman backscattering analyses were performed on crystallographically oriented unpassivated Ge layers. **Fig. 9** shows the normalized Raman spectra obtained from the epitaxial (100)Ge, (110)Ge and (111)Ge layers, depicted in **Fig. 1** (**a1-c1**) along with the bulk (100)Ge substrate. The bulk Ge longitudinal optical (LO) phonon peak mode was measured at $\omega_o \sim 300.21$ cm^{-1}, and any peak shift with respect to this position is considered a strain induced peak shift, where the shift in peak position towards the left is considered to be results of tensile strain and shifts to the right as compressive strain. Since each Ge layer was grown on lattice matched

AlAs buffer layer, no larger (for tensile) or smaller (for compressive) lattice constant stressor was used in these structures, the minute shift in the peak position with respect to ω_o would be due to several factors: thickness of each sample, type of phonon peaks, surface density of atoms for different crystallographically oriented planes, bond strength of atoms on each surface, crystalline homogeneity of each film, phononic vibration of atoms from each crystal plane perpendicular to the surface, *etc*. The full width at half maximum (FWHM) of each Ge layer was evaluated and it was found to be 3.66 cm^{-1}, 4.20 cm^{-1} and 4.79 cm^{-1} for (100)Ge, (110)Ge and (111)Ge, respectively. The FWHM for the bulk Ge (control sample) is 3.26 cm^{-1}. By comparing FWHMs of all epitaxial Ge layers and bulk Ge, one can find that epitaxial (100)Ge is superior compared to the (111)Ge layer since it has a narrower FWHM, closer to the bulk Ge. This can be further corroborated by carrier recombination dynamics *via* μ-PCD technique.

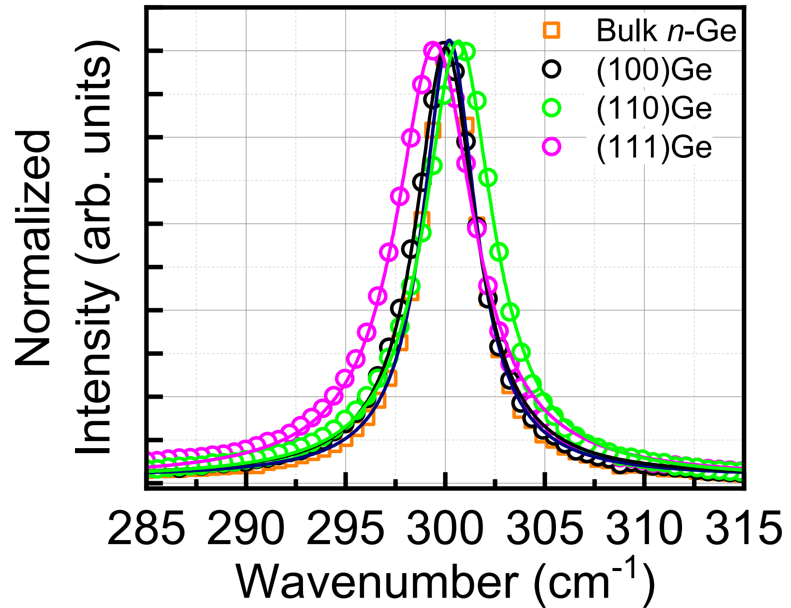

Figure 9. Raman spectra collected from a (100)Ge substrate and crystallographically oriented Ge layers. There is a minute shift of the phonon mode of the oriented Ge layers with respect to the bulk (100)Ge, could be due to the bond strength and surface density of atoms.

3.5. Carrier recombination dynamics of oriented Al_2O_3/Ge heterostructures via μ-PCD. Over the years, carrier lifetimes from semiconductors and their heterostructures[62, 66-69] with (passivated surface) and without passivated surface were estimated to correlate the interface state density with bulk recombination dynamics.[69] The carrier lifetime is strongly dependent on the abundance of defects and dislocations present within the materials. Different carrier lifetime measurement techniques, such as time resolved photoluminescence spectroscopy, *ns*-PCD, μ-PCD, quasi-steady-state PCD to name a few were developed by several researchers over the years.[62, 66-69] In addition, the carrier lifetime was calculated from the current-voltage characteristics of a Ge *pn* junction diode.[49] Furthermore, the carrier lifetime has a strong surface orientation dependence of elementary and binary semiconductors.[50-55] Here,

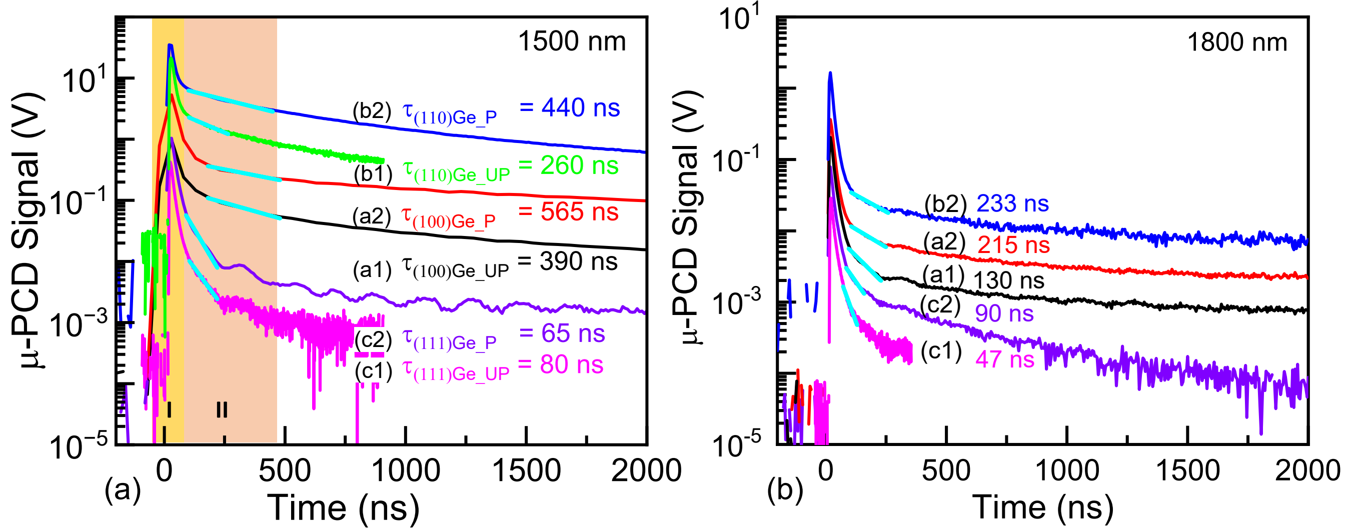

Figure 10. (a) μ-PCD data at 300 K obtained from the crystallographically oriented epitaxial (100)Ge, (110)Ge, (111)Ge layers with (passivated, P: samples **a2**, **b2**, **c2**) and without Al_2O_3 (unpassivated, UP: samples **a1**, **b1**, **c1**) on top grown on respective GaAs substrates with intermediate AlAs buffer layer, wherein the excitation at a 1500 nm wavelength (0.83 eV) was applied from the front side of each heterostructure and the laser power was 20 mW. The figure also shows the fits to the data (Cyan) for each μ-PCD signal, wherein the effective carrier lifetime was determined. **(b)** μ-PCD signal obtained from these heterostructures at 1800 nm (0.69 eV). The measured data has been offset for clarity. The measured lifetime obtained from (111)Ge with or without passivated is way lower than (100)Ge or (110)Ge orientations, indicating either bulk trap states or metallic nature of the (111)Ge layer [54].

the carrier recombination properties in each Al_2O_3/(100)Ge, Al_2O_3/(110)Ge, and Al_2O_3/(111)Ge heterostructure, were probed at room temperature using μ-PCD method at NREL, shown in **Fig. 10**. The two excitation wavelengths of 1500 nm (0.83 eV) and 1800 nm (0.69 eV) with large differences in absorption coefficients (4.7×10^3 cm^{-1} *vs*. 9 cm^{-1}) were selected for both the L and Γ-valley absorption at 1500 nm and only L-valley absorption at 1800 nm. **Fig. 11** shows the schematic representation of the electronic band structure of Ge (0.2% strained) at 0 K (adopted from Ref. [2]) to showcase the selection of the laser excitation during measurement. We assume that the penetration depth at this 1500 nm wavelength is larger than the thickness (280 nm or 290 nm) of Ge layer.

Fig. 10(a) exhibited two-time scale windows, highlighted by the two shaded areas denoting I and II: initial fast decay and steady state decay for carrier recombination. The initial decay process (region I) is due to the excess photogenerated carrier recombination at the surface, and this surface recombination was minimized by depositing ALD Al_2O_3 layer on each Ge sample than sample without Al_2O_3. After surface recombination, photogenerated carriers would diffuse into the bulk of each Ge layer. Excess carriers will recombine quickly for unpassivated Ge

layer due to higher SRV than passivated sample, leading to faster μ-PCD signal decay. This recombination decay is sharper in unpassivated sample than passivated sample, which is expected (*see* slope of fittings, Cyan color) since the carrier recombination would be higher for unpassivated samples. After the initial decay by surface recombination, photogenerated carriers could start to diffuse into the bulk of the Ge layer, however, the rate of diffusion would be significantly lowered for passivated samples except from (111)Ge. The slower time scale (*i.e.,* steady state decay within the bulk of each Ge layer) can be correlated to the bulk lifetime of carriers *via* Shockley-Read-Hall (SRH) recombination, which is associated to carriers trapping on impurities or defect levels within the bulk of each Ge layer. By fitting the measured μ-PCD signal to the mathematical formalism, governed by single exponential function $V_{PCD} = B.exp\left(-\frac{t}{\tau_{PCD}}\right)$, shown in the second shaded area (II) for each heterostructure (Cyan color), the μ-PCD lifetimes (τ_{PCD}) were determined from each oriented Ge layer with Al_2O_3 passivation (P) and unpassivation (UP), *t* is the time, where *B* is a pre-exponential constant. Beyond this region II, there is almost no change in μ-PCD signal with time, and this is referred to the deep into the bulk of semiconductor. The probed carrier lifetime was improved from 390 ns to 565 ns for (100)Ge (improvement ~1.5 ×) and 260 ns to 440 ns for (110)Ge (~1.7 ×) orientations but almost unchanged for (111)Ge after passivation (80 ns *vs.* 65 ns). The wavelength dependent and orientation specific carrier lifetimes along with least square fittings (R^2) value is tabulated in **Table I**. The carrier lifetime from passivated and unpassivated Ge layers were also evaluated at 1800 nm within short fitting ranges and poorer R^2 values (R^2 value close to 1 indicates a good fit).

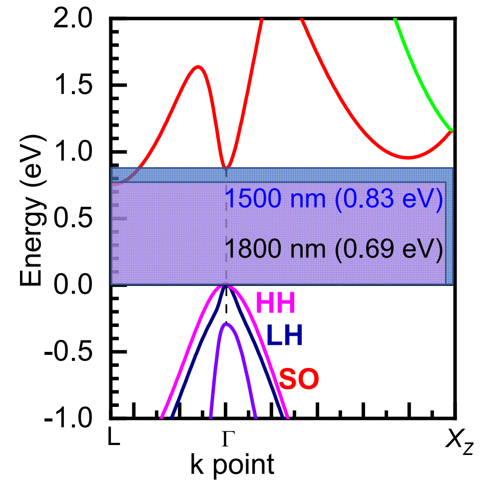

Figure 11. Schematic representation of the electronic band structure of Ge (0.2% strained) at 0 K (adopted from Ref. [2]. At 1500 nm laser excitation, the carriers will redistribute both L and Γ-valleys and at 1800 nm, limited to L-valley absorption, which is very small (~ 9 cm^{-1}) compared to 1500 nm (absorption coefficient ~ 4.7×10^3 cm^{-1}).

Table I. Information on the crystallographically oriented Ge layers and their carrier lifetime.

Sample Label	Orientation	Passivated with Al_2O_3	Lifetime at 1500 nm excitation		Lifetime at 1800 nm excitation		SRV (cm/s)	D_{it} ($eV^{-1}cm^{-2}$)	Ref.
			Lifetime (ns)	R^2	Lifetime (ns)	R^2			
a1	(100) Ge	No	390	0.97953	130	0.96691	316	-	70
a2	Al_2O_3/(100) Ge	Yes	565	0.94547	215	0.98074	100	8.8×10^{11}	30, 39
b1	(110) Ge	No	260	0.98481	-	-	-	-	
b2	Al_2O_3/(110) Ge	Yes	440	0.98226	233	0.9448	-	1.2×10^{12}	30
c1	(111) Ge	No	81	0.97815	47	0.9616	-	-	
c2	Al_2O_3/(111) Ge	Yes	65	0.97555	90	0.94997	-	-	

The measured carrier lifetimes of passivated samples (*see* Table I) were significantly improved over unpassivated samples except for (111)Ge orientation. This implies that the surface recombination velocity stays higher for (111)Ge even after passivation by ALD Al_2O_3. In addition, the (111)Ge could be metallic in nature, as inferred by Tan *et al*.[54] for bulk (111)Ge, and no matter one could do the surface passivation of epitaxial (111)Ge, the carrier lifetime would not be improved. Furthermore, the μ-PCD decay signal is oscillating, and this oscillation could be an artifact of the electronics and cables when connected during measurement that induces impedance mismatch. However, the two technologically important surfaces, (100)Ge and(110)Ge, exhibited high carrier lifetime after Al_2O_3 passivation. The μ-PCD signal at 1800 nm wavelength, shown in **Fig. 10(b)**, quickly drops and the evaluated carrier lifetime for passivated (110)Ge and (100)Ge was 215 ns and 233 ns, respectively, which is almost 50% lower than carrier lifetime measured at 1500 nm wavelength. In addition, the R^2 and fitting ranges for determination of carrier lifetimes were reduced. The low carrier lifetime is due to the lower absorption coefficient at 1800 nm than 1500 nm, which means that direct bandgap nature of Ge *via* strain engineering or incorporation of Sn into Ge is needed for improving carrier absorption.

3.6. Lifetime, SRV, and D_{it} correlation. The surface passivation of Ge by dielectrics such as GeO_2, Al_2O_3, a-Si:H/Al_2O_3, HfO_2, *etc.* can reduce surface recombination by a reduction in D_{it} and the presence of field-effect passivation.[48] Berghuis *et al*[39] used a thin layer of plasma enhanced chemical vapor deposited a-Si:H for chemical passivation and PEALD or thermal ALD Al_2O_3 for field-effect passivation, and demonstrated low SRV of ~2.7 cm/s. In addition, the SRV can be reduced by increasing the thickness of the dielectric layer or an improved field-effect passivation. Here, the surface passivation essentially reduces the surface recombination rate of electrons and holes at the Al_2O_3/Ge heterointerface, and allows more injected carriers to travel through the 280-290 nm thick Ge

layer. The reduced recombination at the Al_2O_3/Ge heterointerface is due to minimizing both SRV and D_{it} that increases the carrier lifetime by diffusing the carriers deep inside the Ge layer. Note that the SRV is a function of injection level of the carriers and here the SRV is applicable to 10^{13} cm^{-3} injection level.

We had estimated the D_{it} from 6.4 nm Al_2O_3/2 nm GeO_x composite gate oxide on (100)Ge/AlAs and (110)Ge/AlAs MOS-Cs as a function of process conditions.[30] The fabricated devices exhibit excellent electrical characteristics with low D_{it} on both (100)Ge and (110)Ge surfaces.[30, 31] Due to the different surface reconstruction of (100)Ge and (110)Ge surface,[59] and oxide compositions (GeO_2 *vs* $Ge_2O_3^-$),[30] the D_{it} levels are slightly different between these orientations. **Table I** shows the measured carrier lifetime, SRV from the literature of unpassivated Ge[42, 70] and Al_2O_3 passivated Ge[39] along with the value of D_{it}.[30] One can find that the carrier lifetime of Al_2O_3 passivated (100)Ge and (110)Ge surfaces are 565 ns at D_{it} of $\approx 8.8\times10^{11}$ $eV^{-1}cm^{-2}$ and 440 ns at D_{it} of $\approx 1.2\times10^{12}$ $eV^{-1}cm^{-2}$, respectively.[30] The SRV values are 316 cm/s[70] and 100 cm/s[39] for (100)Ge surfaces without and with Al_2O_3 passivation, respectively. So, the enhancement of carrier lifetime with Al_2O_3 passivation is mainly due to the reduction of D_{it} compared to unpassivated surfaces of (100)Ge and (110)Ge. On the other hand, the carrier lifetime is almost identical (within the fitting ranges and R^2 value) for unpassivated and passivated (111)Ge surfaces.

3. CONCLUSIONS

Here, crystallographically oriented Ge/AlAs heterostructures were synthesized using solid source molecular beam epitaxy. The core level spectra of atomic species as a function of depth were measured by x-ray photoelectron spectroscopy, revealing no role of orientation effect to the Al_2O_3 dielectric on Ge layers. The charge carrier recombination dynamics of the surface passivated Ge/AlAs heterostructures with atomic layer deposited Al_2O_3 were investigated by microwave photoconductive decay method. The measured carrier lifetimes from passivated Ge/AlAs heterostructures were benchmarked against unpassivated Ge/AlAs heterostructures at an excitation wavelength of 1500 nm with an injection level of ~ 10^{13} cm^{-3}. The carrier lifetimes were significantly improved over unpassivated layers except for (111)Ge orientation. The μ-PCD lifetime was enhanced from 390 ns to 565 ns for (100)Ge (1.5 ×) and 260 ns to 440 ns for (110)Ge (1.7 ×) orientations using Al_2O_3 passivation except for (111)Ge after passivation, showing a strong dependence on surface orientation and passivation due to the lower SRV. High

electrical conductivity of the (111)Ge surface is responsible for low carrier lifetime. Therefore, the enhancement of carrier lifetime of passivated (100)Ge and (110)Ge surfaces due to lower interface defects offers a path for the development of ultra-low power nanoscale transistors.

CONFLICTS OF INTEREST

The authors declare no competing financial interest.

AUTHOR CONTRIBUTIONS

The manuscript was written through contributions of all authors. All authors have given approval to the final version of the manuscript.

AUTHOR INFORMATION

Corresponding Author

*Tel: (540) 231-6663. Fax: (540) 231-3362. E-mail: mantu.hudait@vt.edu.

ORCID

Mantu K. Hudait: 0000-0002-9789-3081

ACKNOWLEDGEMENTS

M. K. H. acknowledge M. Clavel for assisting materials synthesis and ALD dielectrics deposition. Authors also acknowledge P. Goley for TEM measurements. MRD acknowledge Director, CSIR-NEIST Jorhat for the permission for execution of this work. Lastly, the authors are grateful to the Institute for Critical Technology and Applied Science's Nanocharacterization and Fabrication Laboratory, and Virginia Tech Nanofabrication for use of their characterization facilities.

REFERENCES

(1) Clavel, M. B.; Liu, J. -S.; Hudait, M. K. Mapping the Interfacial Electronic Structure of Strain-Engineered Epitaxial Germanium Grown on $In_xAl_{1-x}As$ Stressors. *ACS Omega* **2022**, *7*, 5946-5953.

(2) Hudait, M. K.; Murphy-Armando, F.; Saladukha, D.; Clavel, M. B.; Goley, P. S.; Maurya, D.; Bhattacharya, S.; Ochalski, T. J. Design, Theoretical, and Experimental Investigation of Tensile-Strained Germanium Quantum-Well Laser Structure. *ACS Appl. Electron. Mater.*, **2021**, *10*, 4535-4547.

(3) Saladukha, D.; Clavel, M. B.; Murphy-Armando, F.; Greene-Diniz, G.; Gruening, M.; Hudait, M. K.; Ochalski, T. J. Direct and indirect band gaps in Ge under biaxial tensile strain investigated by photoluminescence and photoreflectance studies. *Phys. Rev.* B **2018**, *97*, 195304-1-12.

(4) Clavel, M. B.; Murphy-Armando, F.; Xie, Y.; Henry, K. T.; Kuhn, M.; Bodnar, R. J.; Khodaparast, G. A.; Smirnov, D.; Heremans, J. J.; Hudait, M. K. Multi-Valley Electron Conduction at the Indirect-Direct Crossover Point in Highly-Strained Germanium. *Phys. Rev. Appl.,* **2022**, *18*, 064083-1-12.

(5) Fang, Y.; Philippopoulos, P.; Culcer, D.; Coish, W. A.; Chesi, S. Recent advances in hole-spin qubits. *Mater. Quantum. Technol.,* **2023**, *3*, 012003-1-28.

(6) Sammak A.; Sabbagh, D.; Hendrickx, N. W.; Lodari, M.; Wuetz B. P.; Tosato, A.; Yeoh, L.; Bollani, M.; Virgilio M.; Schubert M. A.; Zaumseil, P.; Capellini, G.; Veldhorst, M.; Scappucci, G. Shallow and Undoped Germanium Quantum Wells: A Playground for Spin and Hybrid Quantum Technology. *Adv. Functional Materials* **2019**, *29*, 1807613.

(7) Tai, C. -T.; Chiu, P. -Y.; Liu, C. -Y.; Kao, H. -S.; Harris, C. T.; Lu, T. -M.; Hsieh, C. -T.; Chang, S. -W.; Li, J. -Y. Strain Effects on Rashba Spin-Orbit Coupling of 2D Hole Gases in GeSn/Ge Heterostructures. *Adv. Mater.*, ***2021***, *33*, 2007862.

(8) Hudait, M. K.; Johnston, S. W.; Clavel, M. B.; Bhattacharya, S.; Karthikeyan, S.; Joshi, R. High carrier lifetimes in epitaxial germanium-tin/Al(In)As heterostructures with variable tin composition. *J. Materials Chemistry* C **2022**, *10*, 10530-10540.

(9) Olorunsola, O.; Said, A.; Ojo, S.; Stanchu, H.; Abernathy, G.; Amoah, S.; Saha, S.; Wangila, E.; Grant, J.; Acharya, S.; Miller, L.; Rosler, K.; Jheng, Y. -T.; Chang, G. -E.; Li, B.; Salamo, G.; Yu, S. -Q.; Du, W. SiGeSn quantum well for photonics integrated circuits on Si photonics platform: a review. *J. Phys. D: Appl. Phys.,* **2022**, *55*, 443001.

(10) Assali, S.; Attiaoui, A.; Del Vecchio, P.; Mukherjee, S.; Nicolas, J.; Moutanabbir, O. A Light-Hole Germanium Quantum Well on Silicon. *Adv. Mater.*, **2022,** *34* (27), 2201192-1-8.

(11) Elbaz, A.; Buca, D.; von den Driesch, N.; Pantzas, K.; Patriarche, G.; Zerounian, N.; Herth, E.; Checoury, X.; Sauvage, S.; Sagnes, I.; Foti, A.; Ossikovski, R.; Hartmann, J. –M.; Boeuf, F.; Ikonic, Z.; Boucaud, P.; Grützmacher, D.; El Kurdi, M. Ultra-low-threshold continuous-wave and pulsed lasing in tensile-strained GeSn alloys. *Nat. Photonics* **2020**, *14*, 375.

(12) Assali, S.; Dijkstra, A.; Attiaoui, A.; Bouthillier, E.; Haverkort, J. E. M.; Moutanabbir, O. Midinfrared Emission and Absorption in Strained and Relaxed Direct-Band-Gap $Ge_{1-x}Sn_x$ Semiconductors. *Phys. Rev. Appl.,* **2021**, *15*, 024031.

(13) Moutanabbir, O.; Assali, S.; Gong, X.; O'Reilly, E.; Broderick, C. A.; Marzban, B.; Witzens, J.; Du, W.; Yu, S. –Q.; Chelnokov, A.; Buca, D.; Nam, D. Monolithic infrared silicon photonics: The rise of (Si)GeSn semiconductors. *Appl. Phys. Lett.,* **2021**, *118*, 110502.

(14) Morrison, C.; Myronov, M. Strained germanium for applications in spintronics. *Physica Status Solidi (A): Appl. Mater.,* **2016**, *213*, 2809.

(15) Fadaly, E. M. T.; Dijkstra, A.; Renè Suckert, J.; Ziss, D.; van Tilburg, M. A. J.; Mao, C.; Ren, Y.; van Lange, V. T.; Korzun, K.; Kölling, S.; Verheijen, M. A.; Busse, D.; Rödl, C.; Furthmüller, J.; Bechstedt, F.; Stangl, J.; Finley, J. J.; Botti, S.; Haverkort, J. E. M.; Bakkers*,* E. P. A. M. Direct-bandgap emission from hexagonal Ge and SiGe alloys. *Nature* **2020**, *580*, 205-209.

(16) Sharan, N.; Shaik, K. A.; Jang, D.; Schuddinck, P.; Yakimets, D.; Garcia Bardon, M.; Mitard, J.; Arimura, H.; Bufler, F. M.; Eneman, G.; Collaert, N.; Parvais, B.; Spessot, A.; Mocuta, A. Ge Devices: A Potential Candidate for Sub-5-nm Nodes? *IEEE Trans. Electron Dev.*, **2019**, *66*, 4997-5002.

(17) Ye, P.; Ernst, T.; Khare, M. V. The last silicon transistor: Nanosheet devices could be the final evolutionary step for Moore's Law. *IEEE Spectrum* **2019**, 56, 30–35.

(18) Chu, C. -L.; Luo, G. L.; Wu, K.; Chen, S. H.; Chen, B. Y.; Wu, W. F.; Yeh, W. K. Stacked Ge Nanosheet GAAFETs Fabrication and Strain Effects Measurement. *VLSI-TSA*, **2020**, pp. 128-129.

(19) Capogreco, E.; Witters, L.; Arimura, H.; Sebaai, F.; Porret, C.; Hikavyy, A.; Loo, R.; Milenin, A. P.; Eneman, G.; Favia, P.; Bender, H.; Wostyn, K.; Dentoni Litta, E.; Schulze, A.; Vrancken, C.; Opdebeeck, A.; Mitard, J.; Langer, R.; Holsteyns, F.; Waldron, N.; Barla, K.; De Heyn, V.; Mocuta, D.; Collaert, First Demonstration of Vertically Stacked Gate-All-Around Highly Strained Germanium Nanowire pFETs. *IEEE Trans. Electron Dev.*, **2018**, *65*, 5145-5150.

(20) Bae, G.; Bae, D. -I.; Kang, M.; Hwang, S. M.; Kim, S. S.; Seo, B.; Kwon, T. Y.; Lee, T. J.; Moon, C.; Choi, Y. M.; Oikawa, K.; Masuoka, S.; Chun, K. Y.; Park, S. H.; Shin, H. J.; Kim, J. C.; Bhuwalka, K. K.; Kim, D. H.; Kim, W. J.; Yoo, J.; Jeon, H. Y.; Yang, M. S.; Chung, S. -J.; Kim, D.; Ham, B. H.; Park, K. J.; Kim, W. D.; Park, S. H.; Song, G.; Kim, Y. H.; Kang, M. S.; Hwang, K. H.; Park, C. -H.; Lee, J. -H.; Kim, D. -W.; Jung, S. -M.; Kang, H. K. 3 nm GAA Technology featuring Multi-Bridge-Channel FET for Low Power and High-Performance Applications. *IEEE IEDM Tech. Dig.*, Dec. **2018**, p. 28.

(21) Joshi, R.; Karthikeyan, S.; Hudait, M. K. Germanium Nanosheet-FETs Scaled to Sub-nanometer Node Utilizing Monolithically Integrated Lattice Matched Ge/AlAs and Strained Ge/InGaAs. *IEEE Trans. Electron. Dev.*, **2023**, *70*, 899-907.

(22) van Dal, M. J. H.; Vellianitis, G.; Duriez, B.; Doornbos, G.; Hsieh, C. -H.; Lee, B. -H.; Yin, K. -M.; Passlack, M.; Diaz*,* C. H. Germanium p-Channel FinFET Fabricated by Aspect Ratio Trapping. *IEEE Trans. Electron Dev*., **2014**, *61*, 430-436.

(23) Goley, P.; Hudait, M. K. Germanium Based Field-Effect Transistors: Challenges and Opportunities. *Materials* **2014**, *7*, 2301-2339.

(24) Afanas, V. V.; Fedorenko, Y. G.; Stesmans, A. Interface traps and dangling-bond defects in (100)Ge/HfO_2. *Appl. Phys. Lett.*, **2005**, *87*, 032107.

(25) Kuhn, K. J. Considerations for Ultimate CMOS Scaling. *IEEE Trans. Electron Dev.*, **2012**, *59*, 1813-1828.

(26) Agrawal, A.; Barth, M.; Rayner, G. B.; Arun, V. T.; Eichfeld, C.; Lavallee, G.; Yu, S.-Y.; Sang, X.; Brookes, S.; Zheng, Y.; Lee, Y.-J.; Lin, Y.-R.; Wu, C.-H.; Ko, C.-H.; LeBeau, J.; Engel-Herbert, R.; Mohney, S. E.; Yeo, Y.-C.; Datta, S. Enhancement mode strained (1.3%) germanium quantum well FinFET (W_{Fin}=20nm) with high mobility (μ_{Hole}=700 cm^2/Vs), low EOT (~0.7nm) on bulk silicon substrate. *IEEE IEDM Tech. Dig.*, Dec. **2014**, pp. 16.4.1-16.4.4.

(27) Rachmady, W.; Agrawal, A.; Sung, S. H.; Dewey, G.; Chouksey, S.; Chu-Kung, B.; Elbaz, G.; Fischer, P.; Huang, C.Y.; Jun, K.; Krist, B.; Metz, M.; Michaelos, T.; Mueller, B.; Oni, A.A.; Paul, R.; Phan, A.; Sears, P.; Talukdar, T.; Torres, J.; Turkot, R.; Wong, L.; Yoo, H. J.; Kavalieros, J. 300 mm Heterogeneous 3D Integration of Record Performance Layer Transfer Germanium PMOS with Silicon NMOS for Low Power High Performance Logic Applications. *IEEE IEDM Tech. Dig.*, Dec. **2019**, pp. 29.7.1-29.7.4.

(28) Clavel, M.; Bhattacharya, S.; Hudait, M. K. Atomic Layer Deposited Tantalum Silicate on Crystallographically-Oriented Epitaxial Germanium: Interface Chemistry and Band Alignment. *Mater. Adv.,* **2022**, *3*, 5001–5011.

(29) Nguyen, P. D.; Clavel, M. B.; Goley, P. S.; Liu, J.-S.; Allen, N. P.; Guido, L. J.; Hudait, M. K. Heteroepitaxial Ge MOS Devices on Si Using Composite AlAs/GaAs Buffer. *IEEE J. Electron Devices Soc.,* **2015**, *3*, 341–348.

(30) Nguyen, P.; Clavel, M. B.; Liu, J. -S.; Hudait, M. K. Investigating FinFET Sidewall Passivation Using Epitaxial (100)Ge and (110)Ge Metal-Oxide-Semiconductor Devices on AlAs/GaAs. *IEEE Trans. Electron Dev.*, **2017**, *64*, 4457 – 4465.

(31) Nguyen, P. D.; Clavel, M. B.; Ghosh, A.; Hudait, M. K. Metal Work Function Engineering on Epitaxial (100)Ge and (110)Ge Metal-Oxide-Semiconductor Devices. *Microelectron. Eng.* **2018**, *199*, 80–86.

(32) Xie, Q.; Deng, S.; Schaekers, M.; Lin, D.; Caymax, M.; Delabie, A.; Qu, X. -P.; Jiang, Y. -L.; Deduytsche, D.; Detavernier, C. Germanium surface passivation and atomic layer deposition of high-k dielectrics—a tutorial review on Ge-based MOS capacitors. *Semicond. Sci. Technol.*, **2012**, *27*, 1–14.

(33) Xu, Y.; Han, G.; Liu, Y.; Wang, Y.; Liu, Y.; Ao, J.; Hao, Y. Ge pMOSFETs with GeO_x Passivation Formed by Ozone and Plasma Post Oxidation. *Nano. Res. Lett.,* **2019***, 14*, 126.

(34) Ke, M.; Takenaka, M.; Takagi, S. Slow Trap Properties and Generation in Al_2O_3/GeO_x/Ge MOS Interfaces Formed by Plasma Oxidation Process. *ACS Appl. Electron Mater.*, **2019**, *1*, 311-317.

(35) Zhang, L.; Li, H.; Guo, Y.; Tang, K.; Woicik, J.; Robertson, J.; McIntyre, P. C. Selective Passivation of GeO_2/Ge Interface Defects in Atomic Layer Deposited High-k MOS Structures. *ACS Appl. Mater. Inter.*, **2015**, *7*, 20499–20506.

(36) Li, X.; Li, A.; Liu, X.; Gong, Y.; Chen, X.; Li, H.; Wu, D. Effect of chemical surface treatments on interfacial and electrical characteristics of atomic-layer-deposited Al_2O_3 films on Ge substrates. *Appl. Surf. Sci.*, **2011**, *257*, 4589.

(37) Kuzum, D.; Krishnamohan, T.; Pethe, A. J.; Okyay, A. K.; Oshima, Y.; Sun, Y.; McVittie, J. P.; Pianetta, P.A.; McIntyre, P. C.; Saraswat, K. C. Ge-Interface Engineering With Ozone Oxidation for Low Interface-State Density. *IEEE Electron Dev. Lett.,* **2008***, 29*, 328.

(38) Berghuis, W. J. H.; Melskens, J.; Theeuwes, R. J.; Macco, B.; Verheijen, M. A.; Kessels, W. M. M. Surface passivation of germanium by atomic layer deposited Al_2O_3 nanolayers. *J. Mater. Res.*, **2021**, *36*, 571–581.

(39) Berghuis, W-J. H.; Melskens, J.; Macco, B.; Theeuwes, R. J.; Black, L. E.; Verheijen, M. A.; Kessels, W. M. M. Excellent surface passivation of germanium by a-Si:H/Al_2O_3 stacks. *J. Appl. Phys.*, **2021**, *130*, 135303.

(40) Isometsä, J.; Fung, T. H.; Pasanen, T. P.; Liu, H.; Yli-koski, M.; Vähänissi, V.; Savin, H. Achieving surface recombination velocity below 10 cm/s in n-type germanium using ALD Al_2O_3. *APL Mater.,* **2021**, *9*, 111113.

(41) Zhang, R.; Yu, X.; Takenaka, M.; Takagi, S. Impact of Channel Orientation on Electrical Properties of Ge p- and n-MOSFETs With 1-nm EOT Al_2O_3/GeO_x/Ge Gate-Stacks Fabricated by Plasma Post oxidation. *IEEE Trans. Electron Dev.,* **2014**, *61*, 3668-3675.

(42) Chen, Y. Y.; Member, S. S.; Chang, H. C.; Member, S. S.; Chi, Y. H.; Huang, C. H.; Liu, C. W. GeO_2 Passivation for Low Surface Recombination Velocity on Ge Surface. *IEEE Electron Dev. Lett.*, **2013**, *34*, 444–446.

(43) Liu, H.; Han, G.; Liu, Y.; Tang, X.; Yang, J.; Hao, Y. High mobility Ge pMOSFETs with amorphous Si passivation: impact of surface orientation. *Nano. Res. Lett.,* **2019***, 14*, 15.

(44) Zhang, R.; Iwasaki, T.; Taoka, N.; Takenaka, M.; Takagi, S. Al_2O_3/GeO_x/Ge gate stacks with low interface trap density fabricated by electron cyclotron resonance plasma postoxidation. *Appl. Phys. Lett.,* **2011**, *98*, 112902.

(45) Schüttauf, J. A.; van der Werf, K. H. M.; Kielen, I. M.; van Sark, W. G. J. H. M.; Rath, J. K.; Schropp, R. E. I. Excellent crystalline silicon surface passivation by amorphous silicon irrespective of the technique used for chemical vapor deposition. *Appl. Phys. Lett.,* **2011**, *98*, 153514.

(46) Hoex, B.; Schmidt, J.; Pohl, P.; van de Sanden, M.C.M.; Kessels, W.M.M. On the *c*-Si surface passivation mechanism by the negative-charge-dielectric. *J. Appl. Phys.,***2008**, *104*, 113703.

(47) Olibet, S.; Vallat-Sauvain, E.; Ballif, C. Model for a-Si:H/c-Si interface recombination based on the amphoteric nature of silicon dangling bonds. *Phys. Rev.* B **2007**, *76*, 035326.

(48) Abrele, A. G.; Glunz, S.; Warta, W. Field effect passivation of high efficiency silicon solar cells. *Solar. Ener. Mater. Solar Cells* **1993**, *29*, 175-182.

(49) W. S. Jung, "Fluorine passivation of defects in germanium devices", *Doctoral thesis* (Stanford University 2014).

(50) Hudait, M. K.; Johnston, S. Probing Crystallographic Orientation-Specific Carrier Lifetimes in Epitaxial Ge/AlAs and InGaAs/InP Heterostructures. *Mater. Adv.,* **2022**, *3*, 5034-5042.

(51) Huang, M. H.; Naresh, G.; Chen, H. –S. Facet-Dependent Electrical, Photocatalytic, and Optical Properties of Semiconductor Crystals and Their Implications for Applications. *ACS Appl. Mater. Inter.,* **2018**, *10*, 4-15.

(52) Tan, C. –S.; Zhao, Y.; Guo, R. –H.; Chuang, W. –T.; Chen, L. –J.; Huang, M. H. Facet-Dependent Surface Trap States and Carrier Lifetimes of Silicon. *Nano Lett.,* **2020**, *20*, 1952-1958.

(53) Tan, C. –S.; Lu, M. –Y.; Peng, W. –H.; Chen, L. –J.; Huang, M. H. Germanium Possessing Facet-Specific Trap States and Carrier Lifetimes. *J. Phys. Chem. C,* **2020**, *124*, 13304-13309.

(54) Tan, C. –S.; Huang, M. H. Density Functional Theory Calculations Revealing Metal-like Band Structures for Ultrathin Germanium (111) and (211) Surface Layers. *Chem. Asian J*., **2018**, *13*, 1972-1976.

(55) Hsieh, P. -L.; Lee, A. -T.; Chen, L. -J.; Huang, M. H. Germanium Wafers Possessing Facet-Dependent Electrical Conductivity Properties. *Angew. Chem.,* **2018**, *130*, 16394-16397.

(56) Kato, M.; Kohama, K.; Ichikawa, Y.; Ichim, M. Carrier lifetime measurements on various crystal faces of rutile TiO_2 single crystals. *Mater. Lett.*, **2015**, *190*, 397-399.

(57) Hsieh, P. -L.; Kumar, G.; Wang, Y. -Y.; Lu, Y. -J.; Chen L. -J.; Michael H. Huang, M. H. Facet-dependent electrical conductivity properties of GaN wafers. *J. Mater. Chem.* C **2021**, *9*, 15354-15358.

(58) Kumar, G.; Chen, Z. -L.; Jena, S.; Michael H. Huang, M. H. Facet-dependent optical and electrical properties of $SrTiO_3$ wafers. *J. Mater. Chem.* C **2023**, *11*, 3885-3888.

(59) Hudait, M. K.; Zhu, Y.; Jain, N.; Hunter, Jr., J. L. Structural, morphological, and band alignment properties of GaAs/Ge/GaAs heterostructures on (100), (110) and (111)A GaAs substrates. *J. Vac. Sci. Technol.* B **2013**, *31*, 011206-1-14.

(60) Clavel, M. B.; Green-Diniz, G.; Gruning, M.; Henry, K. T.; Kuhn, M.; Bodnar, R. J.; Hudait, M. K. Engineering the Interfacial Electronic Structure of Epitaxial Ge/AlAs(001) Heterointerfaces via Substitutional Boron Incorporation: The Roles of Doping and Interface Stoichiometry. *ACS Appl. Electron. Mater.,* **2019**, *1*, 2646 - 2654.

(61) Hudait, M. K.; Clavel, M.; Goley, P.; Xie, Y.; Heremans, J. J. Magnetotransport Properties of Epitaxial Ge/AlAs Heterostructure Integrated on GaAs and Silicon. *ACS Appl. Mater. Inter.,* **2015***, 7*, 22315-22321.

(62) Johnston, S.; Zaunbrecher, K.; Ahrenkiel, R.; Kuciauskas, D.; Albin, D.; Metzger, W. Simultaneous Measurement of Minority-Carrier Lifetime in Single-Crystal CdTe Using Three Transient Decay Techniques. *IEEE. J. Photovolt.*, **2014**, *4*, 1295.

(63) Chia, C. K.; Dong, J. R.; Chi, D. Z.; Sridhara, A.; Wong, A. S. W.; Suryana, M.; Dalapati, G. K.; Chua, S. J.; Lee*,* S. J. Effects of AlAs interfacial layer on material and optical properties of GaAs⁄Ge(100) Epitaxy. *Appl. Phys. Lett.,* **2008**, *92*, 141905.

(64) S. Swaminathan, "Atomic layer deposited high-k gate oxides on germanium: Interface engineering for scaled metal-oxide-semiconductor devices", *Doctoral thesis* (Stanford University, 2010).

(65) Hudait, M. K.; Zhu, Y.; Maurya, D.; Priya, S.; Patra, P. K.; Ma, A.W. K.; Aphale, A.; Macwan, I. Structural and band alignment properties of Al_2O_3 on epitaxial Ge grown on (100), (110) and (111)A GaAs substrates by molecular beam epitaxy. *J. Applied Physics* **2013**, *113*,134311.

(66) Dev, S.; Wang, Y.; Kim, K.; Zamiri, M.; Kadlec, C.; Goldflam, M.; Hawkins, S.; Shaner, E.; Kim, J.; Krishna, S.; Allen, M.; Allen, J.; Tutuc, E.; Wasserman, D. Measurement of carrier lifetime in micron-scaled materials using resonant microwave circuits. *Nat. Commun.,* **2019**, *10*, 1625.

(67) Cornagliotti, E.; Agostinelli, G.; Van Der Heide, J.; Posthuma, N. E.; Beaucarne, G.; Poortmans, J. Extension of QSSPC lifetime measurement to germanium samples. *In Conference Record of the 2006 IEEE 4th World Conference on Photovoltaic Energy Conversion* (IEEE, **2006**), pp. 1869–1871.

(68) Martín, I.; Alcañiz, A.; Jiménez, A.; López, G.; del Cañizo, C.; Datas, A. Application of quasi-steady state photoconductance technique to lifetime measurements on c-Ge substrates. *IEEE J. Photovolt.,* **2020***, 10*, 1068–1075.

(69) D. K. Schroder, "Carrier lifetimes," in Semiconductor Material and Device Characterization (Wiley, **2006**), pp. 389–464.

(70) Swain, B. P.; Takato, H.; Sakata, I. Wet Chemical Surface Passivation of Germanium Wafers by Quinhydrone–Methanol Treatment for Minority Carrier Lifetime Measurements. *Appl. Phys. Exp.*, **2009**, *2*, 105501.

TABLE OF CONTENT FIGURE